

Electron-impact core excitation of SF₆. I. S 2*p*, S 2*s*, and F 1*s* spectroscopy

James T. Francis,¹ Cássia C. Turci,^{1,2} Tolek Tylliszczak,¹ G. Gerson B. de Souza,² Nobuhiro Kosugi,³ and Adam P. Hitchcock¹

¹*Department of Chemistry, McMaster University, Hamilton, Ontario, Canada L8S 4M1*

²*Instituto de Química, Universidade Federal do Rio de Janeiro, 21910-900 Rio de Janeiro, Brazil*

³*Institute for Molecular Science, Myodaiji, Okazaki 444, Japan*

(Received 7 April 1995)

Electron energy-loss spectra (EELS) of SF₆ have been recorded in the region of S 2*p*, S 2*s*, and F 1*s* excitation, using both dipole and nondipole electron-scattering conditions. Impact energies between 700 and 3200 eV and scattering angles between 0° and 30° were used. Relative to dipole EELS or photoabsorption, there are large intensity redistributions in both the S 2*p* and S 2*s* spectra under nondipole conditions. In contrast, the F 1*s* spectrum is essentially the same in near-dipole and nondipole scattering regimes. A higher-order electric multiple S 2*p* spectra feature is observed at 181 eV. It has an unusual multi-peaked line shape whose components are more closely spaced than the typical 1.15-eV S 2*p* spin-orbit splitting. It is attributed to the overlap of several quadrupole-coupled states, which are likely associated with the [S 2*p*(*t*_{1*u*)⁻¹, *t*_{1*u*) configuration. *Ab initio* self-consistent field calculations for various open-shell S 2*p* excited states are used to assist spectral assignments.}}

PACS number(s): 34.80.Gs, 33.20.Rm, 33.70.Ca

I. INTRODUCTION

The electronic structure of sulphur hexafluoride has been a subject of much interest both because of its technological importance [1–4] and because of its unusual spectroscopy. Photoelectron [5–7], valence-shell [8–10], and inner-shell [11–22] photoionization and valence-shell [23] and inner-shell [24–28] electron energy-loss experimental measurements have been performed. In parallel there has been an extensive effort in calculation of the core excitation of SF₆ using both multiple-scattering [29–35] and molecular-orbital [36–38] approaches. The core excitation spectroscopy of SF₆ has been studied intensively because it is a prototype of a number of species in which a central atom is surrounded by a “cage” of electronegative atoms. Its unusual core excitation spectral features are the consequence of a potential barrier. Nefedov [12] and Dehmer [16] proposed the potential barrier concept to explain the “anomalous” intensity distributions observed in the inner-shell electron excitation spectra of “cage molecules” containing highly electronegative ligands such as SF₆, SO₂, and SiF₄. These unusual intensity redistributions consist of the suppression of direct ionization and the enhancement of selected features, both above and below the inner-shell ionization potential (IP). The latter features are attributed to excitations of core electrons into unoccupied molecular orbitals (UMOs) to form states spatially localized inside a potential barrier.

In the potential barrier model, excited states are localized into either the inner-well or outer-well region of the potential space. Figure 1 depicts a one-dimensional model of this phenomenon. The compact virtual valence orbitals are localized in the inner well and thus there is strong spatial overlap with the compact core orbital. If the symmetry is correct, this results in very intense core to valence excitations in dipole-regime electron energy-loss and x-ray photoabsorption spectra. For SF₆, excitations to the *t*_{1*u*) orbital in the S 1*s* and S 2*s* spectra and excitations to the *a*_{1*g*), *t*_{2*g*), and *e*_g orbitals in}}}

the S 2*p* spectrum are of this type. In contrast, spatially extended Rydberg (4*s*, 3*d*, 4*p*, ...) and near-threshold continuum orbitals are excluded from the inner well and “localized” in the outer-well region. This results in poor overlap with the core orbital and thus low spectral intensities for core to Rydberg excitations [8] and for near-threshold core ionization. Although core to Rydberg transitions are suppressed, they are still observed in the core spectra of most “potential barrier” species, either because of “tunneling” through the barrier or because of Rydberg-valence mixing in which the final-state wave function obtains some “inner-well” character [39–44].

Potential barrier effects have also been observed and predicted in the inner-shell spectra of a wide range of molecules which are not cage molecules, particularly unsaturated species such as N₂ and CO [45–48]. For these species, the enhanced intensity of the core to σ^* feature has been attributed to shape resonances that occur at energies where the outgoing core-ionized electron is temporarily trapped by multiple intramolecular scattering by the anisotropic molecular field. The nature of the potential barrier in both cage and noncage species has been the subject of considerable debate [12,16,47–49]. Multiple-scattering *Xα* calculations [29–35,47,48] suggest that the dominant effect is a centrifugal barrier associated with large angular momentum of the ejected photoelectron since the continuum resonances appear at specific energies in selected angular-momentum partial waves of the outgoing electron in the final state.

Molecular-orbital (MO) calculations also predict intensity enhancements associated with the transitions to core excited states that are quasibound in the continuum [50]. In many cases a one-to-one correspondence can be made between the MO and the shape resonance picture. Stöhr [51] has presented a detailed discussion of the relationships among various models for intensity-enhanced core excitation spectral features. It is debatable whether there is a close correspondence between the MO [21] and shape resonance [12,16]

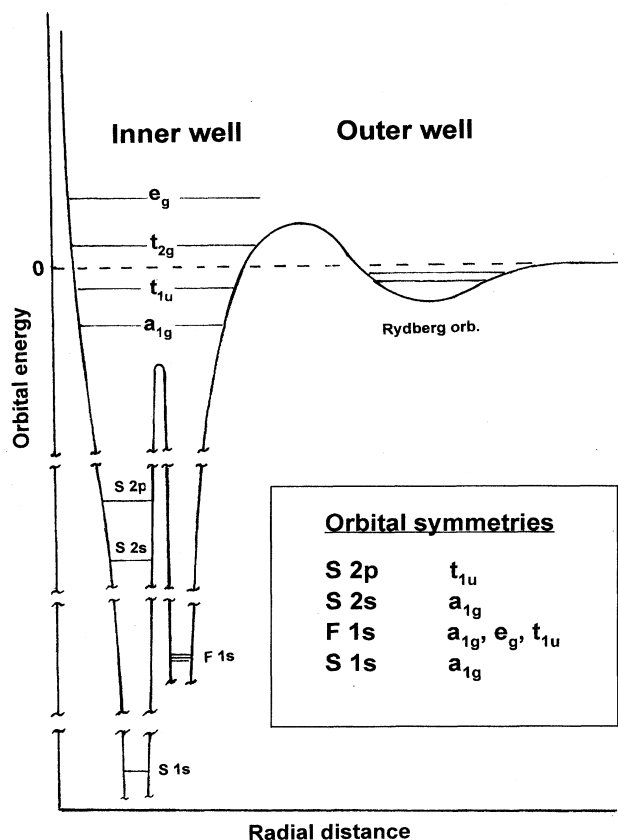


FIG. 1. Schematic of the potential barrier model for core excitation in SF_6 , showing the division of the energy levels into inner-well (occupied core, valence, and virtual valence) and outer-well (Rydberg) components. The one-dimensional potential is fictional. The actual potential will be different for the ground and each excited state.

models for SF_6 . In early studies [12,16] the intensity-enhanced t_{2g} and e_g resonances in the $S\ 2p$ continuum were associated with the t_{2g} and e_g orbitals arising from crystal field splitting of the $S\ 3d$ orbitals. However, Addison-Jones *et al.* [7] have used MS $X\alpha$ calculations to show that similar continuum resonances can be found in a hypothetical octahedral "F₆" species, which does not even contain a S atom. According to the *ab initio* calculations of Reynaud *et al.*, [21], the ligand field splitting of the $S\ 3d$ levels is only 0.04 eV and these levels are bound, not in the continuum. This is consistent with current interpretations of the weak $S\ 2p$ Rydberg signal as involving Rydberg orbitals of primarily $S\ 4s$ and $3d$ character [22]. SF_6 appears to be a case where Robin's concept of Rydberg-valence conjugates [52] applies with the coexistence of states involving both large- R (outer-well) Rydberg $3d$ orbitals and small- R (inner-well) valence $3d^*$ orbitals.

While the electric-dipole core excitation spectroscopy of SF_6 has been very extensively studied, there have been only a few investigations of the nondipole excitations [26,28]. Variable momentum transfer electron energy-loss spectroscopy (EELS) can experimentally investigate excitation mechanisms. The characteristic transition time increases in

small impact parameter, large momentum transfer electron-molecule collisions [53]. Thus it is possible that, in addition to turning on nondipole electronic excitations, there could be large changes to potential barrier phenomena, such as increased intensity of Rydberg and near-continuum transitions. Harrison [26] reported a $S\ 2p$ spectrum recorded with only 74 eV residual energy in which a different spectral feature at 181 eV was clearly observed. Recently Ying, Mathers, and Leung [28] have made a systematic study of the momentum transfer dependence of the $S\ 2p$ spectrum of SF_6 . Owing to the limited resolution and statistics as well as the relatively narrow momentum transfer range that was investigated, Ying, Mathers, and Leung were not able to study the 181-eV state. In order to investigate more completely the nondipole core-excited states of SF_6 , including the different feature at 181 eV, we have carried out a systematic investigation of the $S\ 2p$, $S\ 2s$, and $F\ 1s$ inner-shell electron energy-loss spectra (ISEELS) of SF_6 in both dipole and nondipole scattering regimes. This paper reports our spectroscopic findings, the most significant of which is a detailed investigation of the 181-eV nondipole state. Quantitative generalized oscillator strengths were derived for the $S\ 2p$ spectral features. These values are reported in the following paper [54].

II. METHODOLOGY

A. Experiment

Electron energy-loss spectra of SF_6 in the $S\ 2p$ and $S\ 2s$ regions were measured using a high-resolution energy-loss spectrometer whose design and operation will be described in detail elsewhere. Briefly, a monochromated incident electron beam is focused at a gas jet target. Electrons inelastically scattered at a mechanically determined scattering angle (-10° – 110°) are transported and dispersed using a lens system and a hemispherical electron energy analyzer. The signal is detected using a channel electron multiplier and standard pulse counting electronics. The $F\ 1s$ spectra were recorded using a moderate resolution EELS spectrometer in which the incident electron beam is not monochromated [55].

The sulfur hexafluoride (99.99% purity) used in these experiments was purchased from Matheson and was used without further purification. The overall energy resolution, determined by the monochromator and analyzer pass energies of 70 eV each, was 0.5 eV full width at half maximum (FWHM) for the $S\ 2p$ and $S\ 2s$ experiments carried out with impact energies of 1400 and 1500 eV. For the $S\ 2p$ spectrum recorded with 700 eV impact energy and for $F\ 1s$ spectra recorded on the lower-resolution spectrometer, the resolution was 0.7 eV FWHM. The absolute energy scales were calibrated in the $S\ 2p$ region, using the $S\ 2p_{1/2} \rightarrow t_{2g}$ transition (184.54 eV) reported by Sodhi and Brion [56]; in the $S\ 2s$ region, using the $S\ 2s \rightarrow t_{1u}$ transition (240.5 eV) [25]; and in the $F\ 1s$ region, using the $F\ 1s \rightarrow a_{1g}$ transition (688.0 eV) [25].

B. Calculations

The calculations were carried out using the GSCF3 computer code [57,58] on a MIPS RS3330 UNIX workstation. The core-ionized and core-excited states were obtained by *ab initio* self-consistent field calculations with explicit consider-

TABLE I. S 2*p*, S 2*s*, and F 1*s* core excited states of SF₆. *M*, monopole; *D*, dipole; *Q*, quadrupole; *O*, octupole; *H*; hexadecapole; ?, higher-order multipole $\Delta J > 4$.

Upper orbital	S 2 <i>p</i> (<i>t</i> _{1<i>u</i>}) excitation		S 2 <i>s</i> (<i>a</i> _{1<i>g</i>}) excitation		F 1 <i>s</i> excitation (<i>a</i> _{1<i>g</i>} , <i>t</i> _{1<i>u</i>} , <i>e</i> _{<i>g</i>})		
	State	Selection rule	State	Selection rule	F 1 <i>s</i> orbital	State	Selection rule
6 <i>a</i> _{1<i>g</i>}	<i>T</i> _{1<i>u</i>}	<i>D</i>	<i>A</i> _{1<i>g</i>}	<i>M</i>	2 <i>a</i> _{1<i>g</i>}	<i>A</i> _{1<i>g</i>}	<i>M</i>
					1 <i>t</i> _{1<i>u</i>}	<i>T</i> _{1<i>u</i>}	<i>D</i>
					1 <i>e</i> _{<i>g</i>}	<i>E</i> _{<i>g</i>}	<i>Q</i>
6 <i>t</i> _{1<i>u</i>}	<i>A</i> _{1<i>g</i>}	<i>M</i>	<i>T</i> _{1<i>u</i>}	<i>D</i>	2 <i>a</i> _{1<i>g</i>}	<i>T</i> _{1<i>u</i>}	<i>D</i>
	<i>E</i> _{<i>g</i>}	<i>Q</i>			1 <i>t</i> _{1<i>u</i>}	<i>A</i> _{1<i>g</i>}	<i>M</i>
	<i>T</i> _{1<i>g</i>}	<i>H</i>				<i>E</i> _{<i>g</i>}	<i>Q</i>
	<i>T</i> _{2<i>g</i>}	<i>Q</i>				<i>T</i> _{1<i>g</i>}	<i>H</i>
					<i>T</i> _{2<i>g</i>}	<i>Q</i>	
					1 <i>e</i> _{<i>g</i>}	<i>T</i> _{1<i>u</i>}	<i>D</i>
						<i>T</i> _{2<i>u</i>}	<i>O</i>
2 <i>t</i> _{2<i>g</i>}	<i>A</i> _{1<i>u</i>}	?	<i>T</i> _{2<i>g</i>}	<i>Q</i>	2 <i>a</i> _{1<i>g</i>}	<i>T</i> _{2<i>g</i>}	<i>Q</i>
	<i>E</i> _{<i>u</i>}	?			1 <i>t</i> _{1<i>u</i>}	<i>A</i> _{1<i>u</i>}	?
	<i>T</i> _{1<i>u</i>}	<i>D</i>				<i>E</i> _{<i>u</i>}	?
	<i>T</i> _{2<i>u</i>}	<i>O</i>				<i>T</i> _{1<i>u</i>}	<i>D</i>
					<i>T</i> _{2<i>u</i>}	<i>O</i>	
					1 <i>e</i> _{<i>g</i>}	<i>T</i> _{1<i>g</i>}	<i>H</i>
						<i>T</i> _{2<i>g</i>}	<i>Q</i>
4 <i>e</i> _{<i>g</i>}	<i>T</i> _{2<i>u</i>}	<i>O</i>	<i>E</i> _{<i>g</i>}	<i>Q</i>	2 <i>a</i> _{1<i>g</i>}	<i>E</i> _{<i>g</i>}	<i>Q</i>
	<i>T</i> _{1<i>u</i>}	<i>D</i>			1 <i>t</i> _{1<i>u</i>}	<i>T</i> _{1<i>u</i>}	<i>D</i>
						<i>T</i> _{2<i>u</i>}	<i>O</i>
					1 <i>e</i> _{<i>g</i>}	<i>E</i> _{<i>g</i>}	<i>Q</i>
						<i>A</i> _{2<i>g</i>}	?
						<i>A</i> _{1<i>g</i>}	<i>M</i>

ation of the core hole; i.e., based on the symmetry-adapted Δ SCF method in which the ground and core excited state energies are subtracted to derive excitation energies [59]. Degenerate symmetries of various open-shell S 2*p* excited states were correctly treated, but the spin-orbit interaction was not taken into account. Primitive basis functions were taken from (533/53) and (63/5) or (73/7) contracted Gaussian-type functions of Huzinaga *et al.* [60]. They were augmented with polarization functions for sulfur (1*, $\zeta_d=0.659$ and 0.183) and with tight (compact) functions (1⁺, $\zeta_s=182.0$ and 16.0; $\zeta_p=33.0$; $\zeta_d=6.4$ and 2.1). The tight functions (denoted by 1⁺) account for sulfur orbital contraction upon core hole creation. Without these tight basis functions the orbital relaxation energy upon core hole creation was not sufficiently taken into account and the excitation and ionization energies were overestimated. The contraction schemes were (521211⁺1⁺/411111⁺1⁺1⁺1*1*) and (63/311) for the S 2*p* ionized and excited states, (52121/41111/1*1*) and (721/511/1*) for unionized F atoms, and (411111/31111/1*) for the ionized F atom, with $\zeta_d=1.496$ for the F 1*s* ionized and excited states. Diffuse functions were not included because Rydberg states are not discussed in the present work.

III. RESULTS AND DISCUSSION

A. Orbital and state descriptions

The ground-state electron configuration of SF₆ can be written as follows [61,62]:

Core orbitals

$$(1a_{1g})^2 (2a_{1g})^2 (1t_{1u})^6 (1e_g)^4 (3a_{1g})^2 (2t_{1u})^6$$

S1*s* F1*s* S2*s* S2*p*,

valence orbitals

$$(4a_{1g})^2 (3t_{1u})^6 (2e_g)^4 (5a_{1g})^2 (4t_{1u})^6 (1t_{2g})^6 (3e_g)^4$$

$$\times (1t_{2u})^6 (5t_{1u})^6 (1t_{1g})^6,$$

and virtual valence orbitals

$$(6a_{1g})^0 (6t_{1u})^0 (2t_{2g})^0 (4e_g)^0.$$

Note that, while the ordering of the occupied valence orbitals, in particular the closely spaced 1*t*_{2*u*}, 5*t*_{1*u*}, and 3*e*_{*g*} orbitals, is still a subject of debate, the energy ordering of the virtual valence orbitals is well established, as is the independence of this ordering on the remainder of the electronic configuration.

The states corresponding to the possible configurations arising from excitations of S 2*p*, S 2*s*, and F 1*s* core electrons to the four virtual valence orbitals are summarized in Table I, along with an indication of the order of electric-multipole transition (monopole, dipole, quadrupole, octupole, hexadecapole, or higher-order monopole), which can couple each state to the *A*_{1*g*} electronic ground state. We note that this analysis has been carried out in an *LS*-coupling scheme and thus it ignores the spin-orbit interaction, which

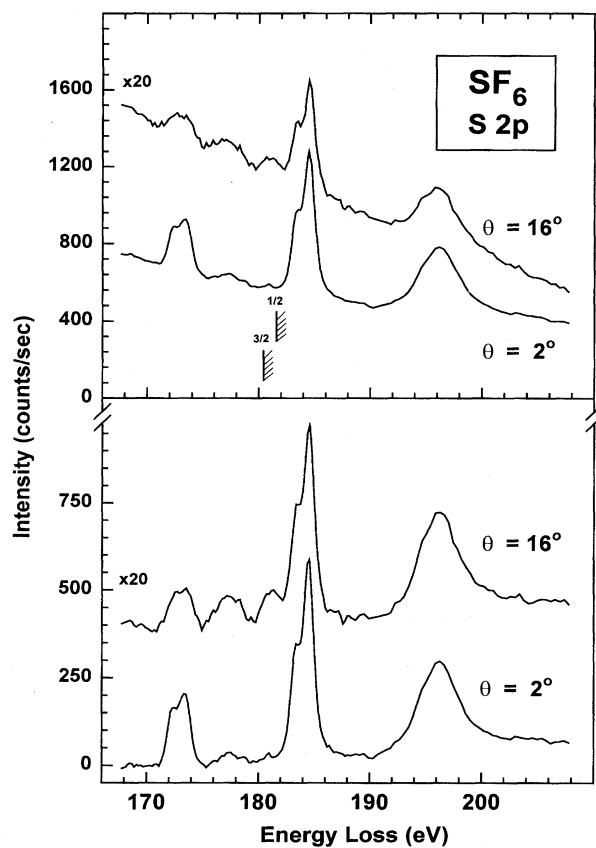


FIG. 2. S 2*p* EELS spectra of SF₆ recorded with 1400 eV impact energy, 2° and 16° scattering angles, and 0.5 eV FWHM instrumental resolution. The top panel plots as-recorded data. The S 2*p* component, isolated by subtraction of an extrapolation of the underlying valence continuum, is plotted in the bottom panel. The 16° spectrum has been multiplied by 20 and offset for clarity. The hatched lines indicate the ionization potential [63,64].

is clearly an important aspect of the S 2*p* spectrum of SF₆ since a spin-orbit splitting of 1.1–1.2 eV is detected in several states.

B. The S 2*p* spectrum

Figure 2 compares ISEELS of SF₆, recorded in the S 2*p* region using dipole ($E_0=1400$ eV, $\theta=2.2^\circ$, $K^2=0.6$ a.u.⁻²) and strongly nondipole ($E_0=1400$ eV, $\theta=16.1^\circ$, and $K^2=8.0$ a.u.⁻²) conditions. Both as-recorded and background-subtracted spectra are presented. The estimated valence-shell signal was generated by extrapolating a least-squares fit of the signal between 155 and 170 eV to a function $a(E-b)^c$. The energies of the S 2*p* spectral features, as well as term values derived using x-ray photoemission spectroscopy (XPS) ionization potentials [63,64], are listed in Table II along with the proposed assignments.

Both synchrotron radiation photoabsorption [12–22] and small-angle EELS [24,25,27] spectra indicate that the dipole-regime S 2*p* spectrum is dominated by three bands, corresponding to dipole-allowed excitations to the a_{1g} , t_{2g} , and e_g virtual valence orbitals. As the group theory analysis in-

TABLE II. Energies (eV), term values, and assignments of features in the S 2*p* electron energy-loss spectrum of SF₆.

Energy loss (±0.1 eV)		Term value (eV)		Assignment
2 <i>p</i> _{3/2}	2 <i>p</i> _{1/2}	2 <i>p</i> _{3/2}	2 <i>p</i> _{1/2}	
172.3	173.4	8.1	8.2	$(t_{1u}^{-1}, 6a_{1g})T_{1u}$
(177.4) ^a		(3.6)		$(t_{1u}^{-1}, 6t_{1u})A_{1g}[\nu(t_{1u})]$
(180.9) ^b		(0.1)		$(t_{1u}^{-1}, 6t_{1u})T_{2g}, E_g^c$
180.4	181.6			IP ^d
183.4	184.5	-3.0	-2.9	$(t_{1u}^{-1}, 2t_{2g})T_{1u}$
(196.2) ^a		(-15.2)		$(t_{1u}^{-1}, 4e_g)T_{1u}$

^aAverage of 3/2 and 1/2. Spin-orbit splitting is not observed; term values are expressed relative to the average IP.

^bAverage peak position. See Fig. 4 and Table III for results of a curve-fit analysis that indicates there are several states and/or a complicated vibronic structure.

^cThe ordering of these states is not clear at present.

^dThe S 2*p* IPs are from XPS measurements [63,64].

icates (Table I), for each of these (S 2*p*⁻¹, UMO) configurations (where umo is the unoccupied MO), there is only a single state that is dipole coupled to the ground state. The main features of the S 2*p* photoabsorption spectra of gaseous and solid SF₆ are identical [15,20], consistent with a dominant, spatially compact, valence character to the excited electron in each of the resonance states. In addition to the dipole-allowed S 2*p* to valence excitations, there are weak Rydberg excitations that are not detected in this work on account of the limited resolution, but that have been well characterized in higher-resolution ISEELS [25,27] and photoabsorption [22] S 2*p* spectra. The Rydberg character of these features is evident from their narrow linewidths as well as their absence from the solid-state spectrum of SF₆ [15,20].

In addition to the dipole signals, there is a broad underlying signal in the 175–178-eV region of the EELS spectrum even at relatively small momentum transfer, which is present but much weaker in the photoabsorption spectrum [22]. The stronger EELS signal has been associated with the quadrupole-allowed, dipole-forbidden S 2*p* → t_{1u} excitation [25], while the weak residue in the optical spectrum has been attributed to electronically forbidden, vibronically allowed-dipole transitions [22]. In the vibronic coupling mechanisms some of the vibrations of the complex (specifically t_{1u} and t_{2u} vibrational modes) distort the octahedral structure in such a way that the center of symmetry is destroyed and thus the combined electronic-vibrational transition becomes allowed within electric-dipole selection rules.

The present dipole-regime spectra are consistent with the earlier EELS results [25,27]. The a_{1g} and t_{2g} features display a spin-orbit doublet structure with a splitting of 1.11(9) and 1.20(3) eV, respectively. The spin-orbit splittings we observe for these states are in agreement (within mutual error bars) with those reported in photoionization studies [7,64]. Figure 3 plots measured spin-orbit separations for the a_{1g} and t_{2g} features, along with the relative intensities of the 2*p*_{3/2} and 2*p*_{1/2} components, as a function of momentum transfer. While fluctuations of up to 0.1 eV are found in the spin-orbit separation, particularly for the a_{1g} state in the intermediate K^2 range where the underlying valence continuum becomes

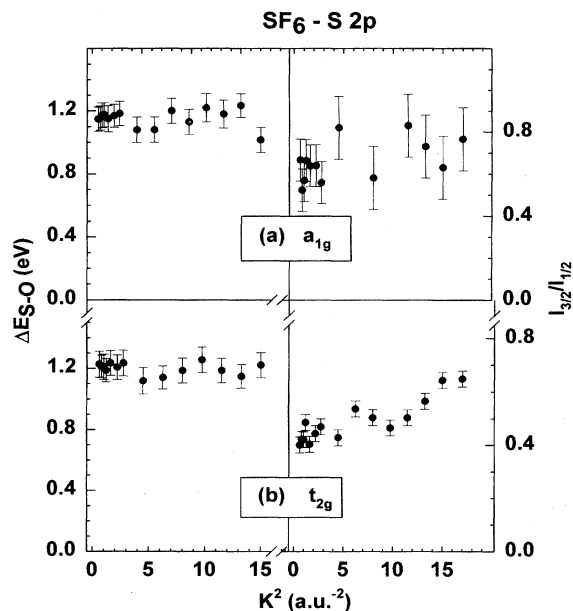


FIG. 3. Magnitude of spin-orbit splitting (ΔE_{s-o} , left panels) and intensity ratio of the 3/2:1/2 components ($I_{3/2}/I_{1/2}$, right panels) for S 2*p* excitation to (a) the a_{1g} and (b) the t_{2g} levels.

very intense producing a very unfavorable S:B ratio [54], the spin-orbit splittings do not change systematically with momentum transfer. In contrast, there are statistically significant changes in the relative intensities of the spin-orbit components of the t_{2g} resonance with momentum transfer. In particular, there is a gradual increase of $I_{3/2}/I_{1/2}$ (ratio of peak areas) from ~ 0.42 to ~ 0.65 for the (S 2*p*⁻¹, t_{2g}) T_{1u} state between 10 and 20 a.u.⁻². Harrison [26] observed that $I_{3/2}/I_{1/2}$ for the " t_{2g} " state increased to approximately 1 when the impact energy was decreased to 225 eV at a scattering angle of 90° ($K^2 \sim 22$ a.u.⁻²). The increase in $I_{3/2}/I_{1/2}$ we observe is consistent with Harrison's observation. Our value of $I_{3/2}/I_{1/2}$ is smaller even though the momentum transfer is similar (greater than 20 a.u.⁻²) because we use a much higher impact energy to achieve a similar K^2 . Thus we are comparing conditions over which the Bethe-Born analysis no longer holds. As we discuss further below, an increase in " $t_{2g}(3/2)$ " relative to " $t_{2g}(1/2)$ " at larger momentum transfer is consistent with the existence of one or more nondipole excitations underlying the dipole-allowed S 2*p*_{3/2} → $t_{2g}(3/2)$ transition.

The linewidths of the a_{1g} , t_{2g} , and e_g resonances are larger than our experimental resolution (0.5 eV) and thus they are controlled by vibrational and/or lifetime broadening effects. For the a_{1g} and t_{2g} states, the linewidth of the S 2*p*_{3/2} component is found to be systematically narrower than that for the S 2*p*_{1/2} component, as previously noted by Hudson *et al.* [22]. This implies a faster core hole decay rate for the S 2*p*_{1/2} states, although the specific decay mechanisms involved remain to be determined by resonant photoemission studies.

At large scattering angles where the momentum transfer increases and nondipole excitations are expected to contribute more strongly, there are dramatic changes in the relative

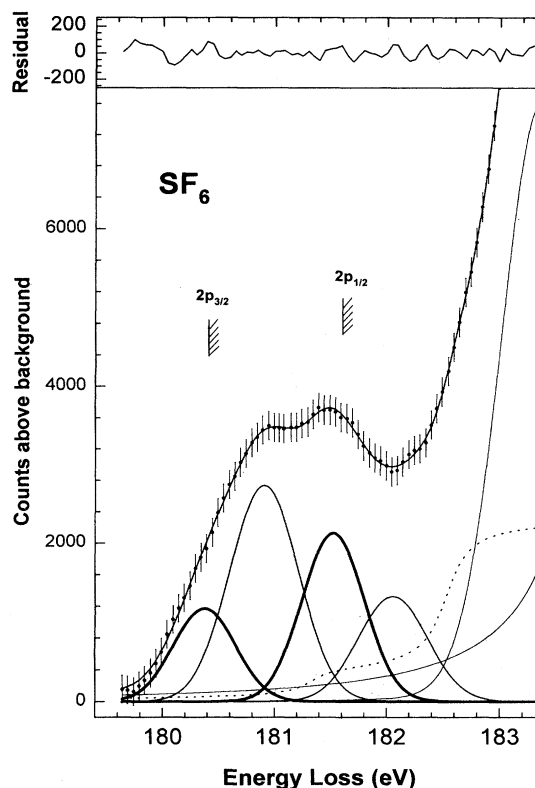


FIG. 4. Expansion of the S 2*p* spectrum of SF₆ in the region of the 181-eV feature, with a curve-fit analysis. The data are the sum of spectra recorded with a resolution of 0.5 eV, impact energy of 1400 eV, and a range of scattering angles between 11° and 21°. The error bars reflect counting statistics. A multipoint smooth was applied to the background subtracted raw data. The upper panel is the residual of the fit, defined as the difference between the smoothed data and the fit. Pairs of lines constrained to have a fixed 1.15-eV separation are indicated by a common line thickness.

intensities of the core to valence excitations. In particular, the intensity of the feature at 177 eV ascribed to S 2*p* → t_{1u} excitations increases considerably with respect to the three dipole-allowed bands. This is consistent with the existence of two excitation mechanisms for this state: the vibronically allowed one, which gives rise to the weak component observed optically, and a nondipole, likely a quadrupole-allowed, mechanism. The intensity of the a_{1g} resonance decreases relative to that of the two strong continuum resonances. In addition to these intensity redistributions, the large scattering angle spectrum clearly exhibits a feature at 181 eV. This signal was first noted by Harrison and King [26], although there are also hints of it in lower momentum transfer EELS spectra [25]. Harrison tentatively attributed this signal to symmetry-forbidden transitions to a state associated with the (S 2*p*_{3/2}⁻¹, t_{2g}) configuration. This assignment was rationalized by the observation of a rather large increase in the intensity of the (S 2*p*_{3/2}⁻¹, t_{2g}) relative to the (S 2*p*_{1/2}⁻¹, t_{2g}) "main line" components in the near-threshold spectrum.

Figure 4 is an expansion of the sum of all nondipole regime, higher-resolution S 2*p* energy loss spectra that exhibit

TABLE III. Results of curve-fit analysis of the 181-eV region of large momentum transfer EELS spectra of SF₆.

Feature	Fit component	Energy (eV)	Intensity ($\times 10^{-2}$)	Width (eV)	Other parameters
$2p_{3/2}$ edge	arctangent	181.33	3.56	0.37 ^a	2.90×10^{-3} ^b decay
$2p_{1/2}$ edge	arctangent	182.53	19.8	0.37 ^a	2.90×10^{-3} ^b decay
nondipole I-3/2	Gaussian	180.38 ^c	11.7	0.65 ^d	
nondipole I-1/2	Gaussian	181.53 ^c	21.3	0.65 ^d	
nondipole II-3/2	Gaussian	180.91 ^c	27.4	0.72 ^f	
nondipole II-1/2	Gaussian	182.06 ^c	13.3	0.72 ^f	
nondipole III-3/2	Gaussian	181.41 ^g	3.46	0.72 ^h	
nondipole III-1/2	Gaussian	182.56 ^g	13.6	0.72 ^h	
$t_{2g}(3/2)$	Voigt	183.36	80.6	0.80	0.060 <i>L</i> fraction
$t_{2g}(1/2)$	Voigt	184.52	305	0.70	0.666 <i>L</i> fraction

^aRequired to have the same value.

^bRequired to have the same value.

^cA fixed 1.15-eV spin-orbit splitting has been imposed on this pair of lines.

^dRequired to have the same value.

^eA fixed 1.15-eV spin-orbit splitting has been imposed on this pair of lines.

^fRequired to have the same value.

^gA fixed 1.15-eV spin-orbit splitting has been imposed on this pair of lines.

^hRequired to have the same value.

the 181-eV feature. Clearly the 0.5-eV separation of the two main components of the 181-eV signal is much too small to correspond to the spin-orbit splitting of a single state. This is evidence that there are two (or more) states each with normal spin-orbit splitting (approximately 1.1 eV) in this energy region that overlap to give rise to the reduced spacing. This spectrum has been fit to the sum of pairs of Voigt and Gaussian lines (constrained to 1.15-eV separation), along with two error-function continua. The positions of the error-function continua were optimized and came about 1 eV higher than the known S $2p$ ionization energies. This was considered appropriate both because of the delayed onset effect and the fact that the maximum cross section of S $2p$ continua lie several eV above the S $2p$ IP. The results of the fit are summarized in Table III. The 181-eV signal clearly has associated substructure, with two main components separated by 0.5(1) eV. In addition, a third component appears necessary to account for the intensity between 182 and 183 eV, although this may be associated either with the use of a symmetric line for the 3/2 component of the t_{2g} resonance or an effect of the shifted IPs.

C. Assignment of the 177- and 181-eV features

The nondipole signal at 181 eV is a rather surprising observation since, in a minimal basis-set *orbital* description, only four S $2p$ excitations to virtual valence levels are expected (see Fig. 1) and these have already been identified. The enhanced intensity of the 181-eV signal with increasing momentum transfer is evidence for either a higher-order electric-multipole or a spin-forbidden transition. Gianturco, Guidotti, and Lumanna [36] have reported a fifth virtual orbital of t_{1u} symmetry, which they distinguish from the ‘‘conventional’’ t_{1u} (S $3p$) orbital in terms of spatial alignment (note that a proper linear combination of atomic orbitals description is not given, so it is difficult to determine exactly the character of their $1t_{1u}$ and $2t_{1u}$ orbitals). They calculate a $1t_{1u}/2t_{1u}$ splitting of only 0.8 eV in the ground state but

much larger values in the core excited states (9 eV in S $2p$, 5 eV in F $1s$, and 10 eV in S $1s$). However, this result is considered to be an artifact of the use of double- ζ functions in the calculational method and the higher energy $2t_{1u}$ orbital does not correspond to any physical observable.

While an *orbital* picture cannot explain the 181-eV feature, when the S $2p$ spectrum is considered from a *state* perspective there are a number of candidate states for which spectral signatures have not been identified. As outlined in Table I, there are 11 states that arise from S $2p$ excitation to the four virtual valence orbitals. Among these, there are two states that are coupled to the ground state via dipole-forbidden, quadrupole-allowed transitions. One possibility is that the features at 177 and 181 eV correspond to these two states, since quadrupole transition matrix elements will generally be larger than higher-order electric-multipole matrix elements. Before adopting this interpretation, we considered a number of alternative possible assignments and the comparison with *ab initio* Δ SCF calculations.

1. Reassignment of the S $2p \rightarrow t_{1u}$ excitation

One possibility is that the conventional assignment of the quadrupole S $2p \rightarrow t_{1u}$ excitation to the 177-eV feature is incorrect and that the 181-eV signal is in fact this one-electron excitation. The 177-eV feature could then be explained in terms of a quadrupole S $2p$ to Rydberg transition, such as one of $2p \rightarrow 4p$ character. However, one can argue rather strongly against this proposal on several grounds. The term value of the 177-eV signal traditionally assigned as the S $2p \rightarrow t_{1u}$ excitation matches well that of the dominant electric-dipole-allowed signal in the S $2s$ and S $1s$ spectra [25]. The breadth of the 177-eV feature is much more characteristic of an excitation to a virtual valence level for which dissociation or extensive vibrational excitation often leads to a broad band, as opposed to excitations to a nonbonding Rydberg orbital, which usually result in sharp, narrow spectral features. Hudson *et al.* [22] have observed a sharp fea-

ture at 178.2 eV, which they have assigned as the vibronically allowed S $2p \rightarrow 4p$ Rydberg transition.

Negative-ion resonance states, which can be detected by electron transmission spectroscopy (ETS) or dissociative electron attachment, provide a probe of unoccupied electronic structure that complements core excitation. ETS and elastic electron scattering studies of SF₆ [65] have identified features attributable to SF₆⁻ states in which the additional electron is located in the a_{1g} , t_{1u} , or t_{2g} orbital. The relative separation of these negative-ion resonances is in good agreement with that of the core excitation term values (see Table VIII). This supports the accepted assignments of the four S $2p$ spectral features. In particular, there is no evidence of an additional feature between those attributed to the t_{1u} and t_{2g} negative-ion states.

2. Triplet partner to the $[t_{1u}(S\ 2p)^{-1}, t_{2g}]$ state

The 181-eV signal is about 2 eV below that of the main t_{2g} resonance. This separation is a plausible magnitude for a singlet-triplet exchange splitting especially since large singlet-triplet splittings are generally associated with intense spin-conserving singlet excitations [66]. However, the analogy with species obeying LS coupling is imprecise. The angular-momentum coupling in SF₆ should be dealt with in a manner intermediate between LS and jj coupling. The separation of the 3/2 and 1/2 components of the $[t_{1u}(S\ 2p)^{-1}, t_{2g}]$ state in (jj) coupling is closely related to the singlet-triplet splitting in an LS -coupling picture. Thus this possibility can be ruled out from first principles. Even so, we have recorded the S $2p$ spectrum with only 700 eV impact energy in order to seek any additional states that might appear under these conditions. Lowering the impact energy is more effective than increasing the scattering angle for enhancing spin-exchange excitations [66]. Figure 5 illustrates how the 181-eV and " t_{2g} " signals change with increasing scattering angle ($20^\circ \rightarrow 30^\circ$ at $E_0 = 1400$ eV) and decreasing impact energy (1400 eV \rightarrow 700 eV). Relative to the t_{2g} peak, the 181-eV signal is *less intense* at 700 eV than at 1400 eV impact energy, even though the scattering angles were chosen to have approximately the same K^2 value. This is rather strong evidence against any involvement of a spin exchange process in generating the 181-eV feature. On the other hand, the systematic increase in intensity with increasing momentum transfer [54] is fully consistent with a spin-conserving electric-quadrupole- (or higher-order electric-multipole-) allowed transition.

3. Quadrupole transition to a double excitation state

While two-electron (core to valence plus valence to valence) excitations are generally rather weak, the inner-well localized character of the S $2p$ excited states could considerably enhance the intensity of a quadrupole-allowed double excitation. Plausible candidates would need to combine the highest occupied to lowest unoccupied molecular-orbital ($t_{1g} \rightarrow a_{1g}$) excitation with the S $2p \rightarrow a_{1g}$ excitation. The lowest-energy electronic excited state of SF₆ is 9.6 eV and thus the lowest likely double excitation at 173 + 9.6 eV, or 182.6 eV. This is 1.6 eV above the 181-eV signal and since double excitation energies are usually larger than those estimated from the sum of single excitation energies, a quadrupole double excitation is not a plausible interpretation.

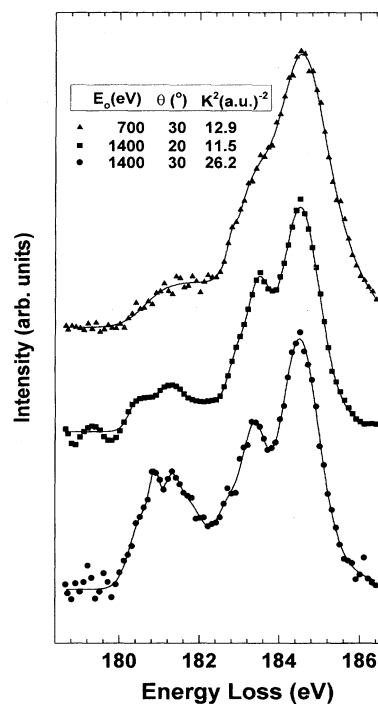


FIG. 5. Comparison of S $2p$ spectra of SF₆ in the region of the 181-eV feature, recorded at 700 eV, 30°; 1400 eV, 20°; and 1400 eV, 30°; impact energy and scattering angles, conditions corresponding to K^2 values of 12.9, 11.5, and 26.2 a.u.⁻², respectively. The solid line is the result of a curve fit to the data using a set of lines similar to that used for the fit plotted in Fig. [4].

4. Enhanced threshold ionization signal at large momentum transfer

When the 181-eV region is subjected to a curve-fit analysis (see Fig. 4), there are lines with onsets close to the S $2p$ IPs of 180.4 and 181.6 eV [63,64]. This led us to consider enhanced tunneling of very-low-energy electrons into the direct ionization channel as a possible explanation. Since the *time* for a large momentum transfer scattering event is much larger than that of a grazing, low momentum transfer collision [53], the probability for tunneling could plausibly increase. However, if this was the case at threshold, it is difficult to understand why the continuum intensity would not be enhanced at all energies up to the top of the barrier (which loosely can be taken as lying around 192 eV, the onset of the second fitted continuum [54]). While the intensity of the lower-energy portion of the S $2p$ continuum (180.4–190 eV) does increase at increasing momentum transfer, there is a large difference between the momentum transfer dependence for the 181-eV peak and the underlying 180–190-eV continuum signal. It is possible that the 181-eV signal corresponds to a component of the direct ionization, which is additionally enhanced at threshold through a combination of post-collision interaction (PCI) effects [67] and increased interaction time. Photoemission or electron-electron coincidence spectroscopy close to threshold [68] might reveal direct evidence for a PCI-like effect, in terms of shifts in the photoelectron energies. In the absence of direct evidence of this type we do not support such a speculative interpretation.

TABLE IV. Results of *ab initio* Δ SCF calculations for various open-shell S $2p$ excited states of SF₆.

Orbital	State	S $2p$ (triplet)		S $2p$ (singlet)		ΔE_{s-o} (eV)	Optimum coupling ^b
		E (eV)	(TV) ^a	E (eV)	(TV) ^a		
$6a_{1g}$	T_{1u}	174.57	(7.89)	175.18	(7.28)	0.61	<i>jj</i>
$6t_{1u}$	A_{1g}	179.44	(3.02)	185.25	(-2.79)	5.81	<i>LS</i>
$6t_{1u}$	T_{2g}	180.50	(1.96)	181.07	(1.39)	0.57	<i>jj</i>
$6t_{1u}$	E_g	180.51	(1.95)	181.20	(1.26)	0.69	<i>jj</i>
$2t_{2g}$	T_{1u}	184.89	(-2.43)	185.75	(-3.29)	0.86	<i>jj</i>
$2t_{2g}$	T_{2u}	185.09	(-2.63)	185.62	(-3.16)	0.53	<i>jj</i>
$4e_g$	T_{1u}	195.96	(-13.50)	197.21	(-14.75)	1.25	intermediate

^aTV is equal to the term value (IP- E). Calculated relative to calculated IP of 182.46 eV.

^bWhen the singlet-triplet separation is larger than the spin-orbital splitting (1.15 eV) the *LS*-coupling approach is better. Conversely, when the singlet-triplet separation is smaller than the spin-orbit splitting (1.15 eV) the *jj*-coupling approach is better.

D. *Ab initio* calculations for S $2p$ excitation

The results of the *ab initio* Δ SCF calculations are summarized in Table IV. In addition to providing a good match to the strong dipole excitations (compare Tables II and IV), the calculation indicates that the states derived from the (S $2p^{-1}, t_{1u}$) configuration span an energy range as large as 6 eV. In particular they indicate that the ${}^3A_{1g}$ state lies significantly lower in energy than the ${}^{1,3}T_{2g}$ and ${}^{1,3}E_g$ states. The T_{2g} and E_g states are predicted to occur at the same energy and to have a much smaller singlet-triplet splitting than the A_{1g} state. This suggests that the 177-eV signal observed weakly by photoabsorption is the *jj* or intermediate coupling equivalent to the ${}^3A_{1g}$ state, which is vibronically allowed on account of simultaneous excitation of a t_{1u} vibration. Presumably “intensity borrowing” occurs from the intense $T_{1u}(S\ 2p^{-1}, t_{2g})$ resonance at 184 eV. The 181-eV state would then be attributed to the overlap of the quadrupole-allowed, dipole-forbidden T_{2g} and E_g states. The complex line shape we observe for the 181-eV signal could then be attributed to a combination of the existence of the two states in a narrow energy range, combined with likely Jahn-Teller splittings of these degenerate states. Since the calculation places the octupole-coupled T_{2u} state of the (S $2p^{-1}, t_{2g}$) configuration above the $T_{1u}(S\ 2p^{-1}, t_{2g})$ state, the calculation does not support the assignment of the 181-eV feature proposed by Harrison [26].

This interpretation nicely explains the presence of the 177-eV signal but not the 181-eV signal in optical spectra. It places emphasis on the low-lying ${}^3A_{1g}$ state to explain the 177-eV state. Although excitations to this state are orbital forbidden, they are more or less spin allowed through the spin-orbit interaction (intermediate coupling) that couples the ${}^3A_{1g}$ and ${}^1A_{1g}$ states. The calculation does not explain the enhanced intensity of the 177-eV signal at increasing momentum transfer. It is possible that the transition to the ${}^3A_{1g}(S\ 2p^{-1}, t_{1u})$ state increases in intensity with increasing momentum transfer, although this would be rather unusual for a (vibronically) dipole-coupled state, particularly when the state from which intensity is borrowed is decreasing in intensity. Alternatively, the calculations, which are not relativistic and thus do not correctly account for all aspects of angular-momentum coupling, may be in error with regard to the relative energies of the quadrupole-allowed, dipole-forbidden T_{2g} and E_g states. It is possible that one of these

contributes at 181 eV and the other at 177 eV.

Based on the above considerations, we believe the 181-eV feature corresponds to several higher-order electric-multipole transitions, such as the $T_{2u}[S\ 2p(t_{1u})^{-1}, t_{2g}]$ octupole-allowed state as suggested by Harrison [26] and/or the two quadrupole-coupled T_{2g} and E_g states associated with the $[S\ 2p(t_{1u})^{-1}, t_{1u}]$ configuration. While we also observe some increase in the $t_{2g}(3/2)$ intensity, which was Harrison’s experimental basis for suggesting the $T_{2u}[S\ 2p(t_{1u})^{-1}, t_{2g}]$ assignment, we prefer an assignment in terms of the E_g or T_{2g} states arising from the $[S\ 2p(t_{1u})^{-1}, t_{1u}]$ configuration. There are four reasons for this. First, we see only a small increase in the $t_{2g}(3/2)$ intensity even at similar K^2 values (see Fig. 3). Both the experimental data and the curve-fit analysis require relatively little contribution of “181-eV signal” underlying the $t_{2g}(3/2)$ line, in contrast to the observations of Harrison. Second, we partially resolve the 181-eV signal into several components and deduce the presence of at least two states with reasonable spin-orbit splittings (see Fig. 4). This indicates that there are contributions from two non-dipole states, arising from either the (S $2p^{-1}, t_{1u}$) or (S $2p^{-1}, t_{2g}$) configuration. Third, from the Bethe-Born expansion [54], quadrupole states should appear before octupole states as the momentum transfer increases. Fourth, our calculations (Table IV) predict an average term value of 1.9 eV for the (S $2p^{-1}, t_{1u}$) states. This value (as well as that of 1.8 eV predicted by Tossell [69]) is in good agreement with the *average* of the energies of the 177- and 181-eV features attributed to the $[S\ 2p(t_{1u})^{-1}, t_{1u}]$ configuration, but it is in significant disagreement with the term value for the 177-eV state alone.

Overall, the picture that arises from the combination of experiment and theory is that the 177-eV feature has both a dipole-allowed and a dipole-forbidden component, with the dipole-allowed component arising from vibronic coupling and Jahn-Teller distortion, with intensity borrowed from the strong t_{2g} excitation, as suggested by Hudson *et al.* [22]. The origin of the dipole-forbidden component of the 177-eV signal is not clear at present. The 181-eV feature arises from several nondipole excitations, one of which is the quadrupole S $2p \rightarrow t_{1u}$ excitation, the other(s) of which could be either another quadrupole state from S $2p \rightarrow t_{1u}$ excitation or the octupole T_{2u} state associated with S $2p \rightarrow t_{2g}$ excitation.

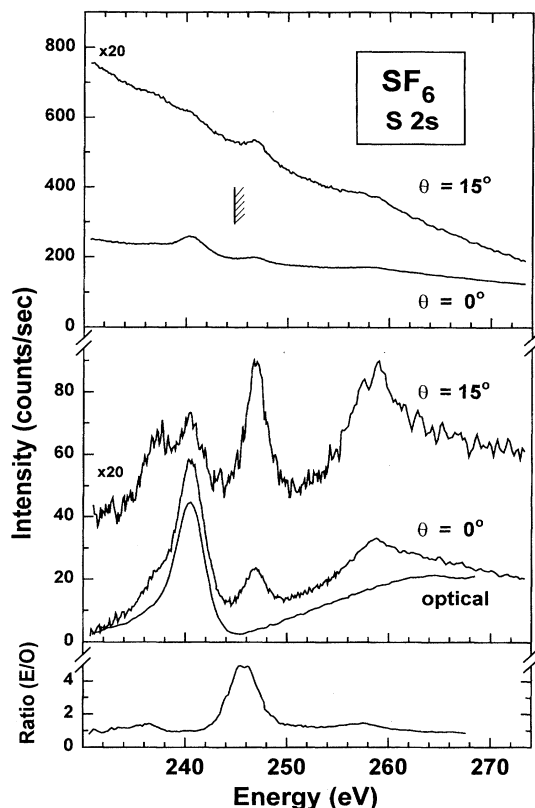


FIG. 6. S 2s EELS spectra of SF₆ recorded with 1500 eV impact energy and the indicated angles. The top panel plots the as-recorded spectra. The S 2s components isolated by the subtraction of an extrapolation of the underlying S 2p continuum are displayed in the central panel, in comparison to the optical (total ion yield) spectrum. The 15° spectrum has been multiplied by 20 and offset for clarity. The lower panel displays the ratio of the 0° EELS to the optical data. The values greater than unity at 236, 246, and 258 eV are clear indications of nondipole contributions. The hatched line indicates the S 2s ionization potential [64].

Clearly, further theoretical work is needed to make a definitive assignment.

E. The S 2s spectrum

Figure 6 compares ISEELS of SF₆ in the S 2s region, recorded using both “near-dipole” ($E_0=1500$ eV, $\theta=0^\circ$) and strongly nondipole ($E_0=1500$ eV, $\theta=15^\circ$) conditions. For each spectrum, both as-recorded and background subtracted data are presented. In addition, a background subtracted S 2s optical (total photoion yield) spectrum is presented, along with the ratio of the near-dipole and optical spectra. Since the S 2s signal is relatively weak and the underlying S 2p continuum intensity quite strong, very good quality data are required to allow examination of the S 2s spectra with adequate statistics. The energies of the S 2s spectral features as well as term values derived using XPS ionization potentials [64] are listed in Table V along with the assignments.

As outlined in Table I and noted in many previous discussions of the core spectroscopy of SF₆, there is a complimen-

TABLE V. Energies (eV), term values, and assignments of features in the S 2s electron energy-loss spectrum of SF₆.

Energy loss (± 0.1 eV)	Term value (eV)	Energy loss ^a	Assignment
237.3	7.4	236.9	(S 2s ⁻¹ , 6a _{1g})A _{1g}
240.5	4.2	240.5	(S 2s ⁻¹ , 6t _{1u})T _{1u}
244.7		244.7	IP ^b
246.9	-2.2	246.7	(S 2s ⁻¹ , 2t _{2g})T _{2g}
258.9	-14.2	259.0	(S 2s ⁻¹ , 4e _g)E _g

^aFrom [27].

^bFrom XPS [64].

tary between the selection rules for S 2p and S 2s excitation. Excitation to levels that are dipole allowed from S 2p are dipole forbidden from S 2s and vice versa. Thus the only electric-dipole-allowed inner-well core to valence transition is that to the (S 2s⁻¹, t_{1u})T_{1u} state. Photoabsorption spectra [7,14] detect only this feature (see Fig. 6). In contrast, even in the dipole scattering regime, EELS spectra exhibit relatively strong contributions from dipole-forbidden, quadrupole-allowed S 2s excitations to the t_{2g} and e_g orbitals. Careful examination of the 0° spectrum reveals a weak shoulder at 239 eV, which is particularly evident in the comparison to the optical spectrum (Fig. 6). This feature is a weak S 2s → a_{1g} excitation. Also, the features at 247 and 259 eV, ascribed to nondipole excitations to the t_{2g} and e_g orbitals, are relatively prominent even in the lower momentum transfer spectrum. This indicates that excitations from 2s core levels have relatively more intense nondipole transitions than excitations from S 2p levels. This parallels observations of large nondipole contributions in 2s and 3s energy-loss spectra of solids [70] and surfaces [71,72], even under conditions where the 2p or 3p spectra are essentially at the optical limit.

At large momentum transfer conditions the intensity of all S 2s features declines relative to the underlying S 2p ionization continuum. This makes it difficult to detect the weak signal on a strong background, but a reasonable quality spectrum was achieved at 15° scattering angle after 150 h of signal averaging. This spectrum exhibits a great increase in intensity of the quadrupole excitations to the a_{1g}, t_{2g}, and e_g orbitals, with the most dramatic change being the clear detection of the a_{1g} feature at 237 eV. In contrast to the S 2p spectrum, at larger momentum transfer the nondipole components become more intense than the dipole components.

F. The F 1s spectrum

Figure 7 compares ISEELS of SF₆ in the F 1s region, recorded on a lower-resolution spectrometer under near-dipole ($E_0=3200$ eV, $\theta \approx 2-4^\circ$, and $3.3 < K^2 < 4.2$ a.u.⁻²) and nondipole ($E_0=1500$ eV, $\theta \approx 8-10^\circ$, and $8.1 < K^2 < 10.5$ a.u.⁻²) scattering conditions. A linear background has been subtracted from both spectra. The energies of the F 1s spectral features as well as term values derived using XPS ionization potentials [64] are listed in Table VI along with the spectral assignments.

While a superficial examination of the F 1s spectrum suggests that there are four resonances corresponding to F 1s

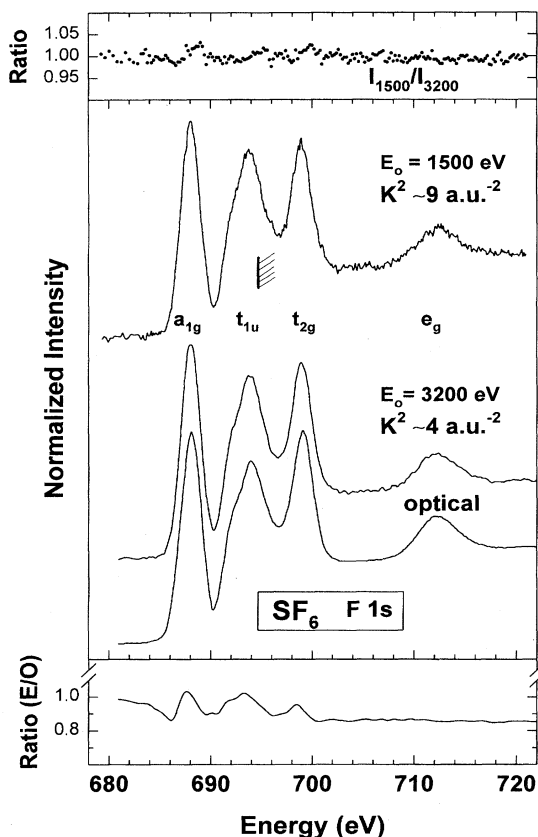


FIG. 7. F 1s EELS spectra of SF₆ recorded with 1500 eV impact energy (8°–10°) and 3200 eV impact energy (2°–4°), compared to the optical photoionization yield spectrum [22]. The background subtracted optical data have been scaled to match the energy-loss data between 680 and 692 eV. The upper panel is the ratio of the two energy-loss spectra while the lower panel is the ratio of the energy-loss and optical spectra. The hatched line indicates the F 1s ionization potential [64].

excitations to the four virtual valence orbitals, a closer examination reveals a distinct shoulder on the second peak, with an energy of 692.4 eV, 1.6 eV below the peak maximum at 694.0 eV. A consideration of the F 1s core excited states (Table I) indicates there are five F 1s excited states that are dipole coupled to the ground state. It is logical to assign

TABLE VI. Energies (eV), term values, and assignments of features in the F 1s electron energy-loss spectrum of SF₆.

Energy loss (±0.2 eV)	Term value (eV)	Assignment
688.0	6.6	(1t _{1u} , 6a _{1g})T _{1u}
692.4 (sh) ^b	2.2	(2a _{1g} , 6t _{1u})T _{1u}
694.0	0.6	(1e _g , 6t _{1u})T _{1u}
694.6		IP ^a
698.9	-4.3	(1t _{1u} , 2t _{2g})T _{1u}
712.1	-17.5	(1t _{1u} , 4e _g)T _{1u}

^aFrom XPS [64].

^bsh denotes shoulder.

the two dipole-coupled states, $T_{1u}(2a_{1g}, 6t_{1u})$ and $T_{1u}(1e_g, 6t_{1u})$, to the two parts of the second peak. While there is relative little difference (less than 0.2 eV) in the binding energies of the three F 1s orbitals, there must be differences in electron-electron repulsion and configuration interactions among the (F 1s, t_{1u}) states in order to give rise to a 1.6-eV splitting.

Table VII summarizes the results of *ab initio* calculations of the F 1s → t_{1u} excitation carried out with a localized core hole. In this picture, the lower-energy state is associated with excitations to t_{1u}(z), the component of the t_{1u} UMO oriented in the same direction as the bond between the central sulfur atom and the core excited fluorine atom, while the higher-energy state is associated with excitations to t_{1u}(x,y), the component oriented in the two orthogonal directions. When one considers linear combinations of these localized core excited states to form correctly symmetry-adapted states in the O_h point group, it turns out there is no simple correspondence between the t_{1u}(z) and t_{1u}(x,y) localized states and the T_{1u}(2a_{1g}, 6t_{1u}) and T_{1u}(1e_g, 6t_{1u}) delocalized states (see Table VII). The localized core hole calculation predicts relative amplitudes (1:3) similar to experiment and a predicted separation (1.13 eV) that is about two-thirds of that observed (1.6 eV). It is noteworthy that, in addition to clarifying an aspect of the F 1s spectrum of SF₆, this improved analysis of the dipole components of the F 1s spectrum lends support to our proposal with regard to the nondipole S 2p → t_{1u} excitations, by showing unambiguously that there can be significant energy splittings among different states associated with the same configuration.

In order to check for nondipole F 1s excitations we have examined the changes in the spectrum with increasing momentum transfer as well as making a direct comparison to optical (total ionization yield) data [22]. The ratio of the two energy-loss signals (top panel of Fig. 7) is essentially unstructured, indicating very little momentum transfer dependence of the spectral shape. The scale of the optical data has been chosen to provide a match of the background-subtracted intensity to the 3200-eV ISEELS data at the a_{1g} resonance. With this choice of scaling, the ratio of the lower momentum transfer energy-loss spectrum to the optical spectrum (bottom panel of Fig. 7) shows near unit values at the a_{1g} and t_{1u} resonances (as expected from the choice of scaling). The structure in the ratio curve is along the rise and fall of the resonances and is likely related to differences in resolution. There is a relatively abrupt decline by 15% in the ratio at the F 1s ionization energy (694.6 eV). We believe this is an artifact associated with an enhanced sensitivity to core ionization relative to core excitation when using total ionization detection of optical absorption [74]. While the momentum transfer even with 3200 eV impact energy is ~4 a.u.⁻², which is sufficient for there to be nondipole contributions, both the independence of the spectral shape with impact energy and the similarity to the optical data strongly suggest there are no significant contributions from nondipole excited states in the regime of momentum transfer examined.

In the S 2p and S 2s edges there is a clear enhancement of the intensity of transitions to dipole-forbidden states with increasing momentum transfer. However, there is little or no change in the F 1s spectral shape with increasing momentum transfer. The dominance of dipole translations is likely related to the fact that there are electric-dipole excitations from

TABLE VII. F 1s excitations predicted by *ab initio* Δ SCF calculations based on a localized core hole model. (a) Calculated energies. (b) Localized descriptions. There are 6 F atoms, $F+x$, $F-x$, $F-y$, $F+z$, and $F-z$. There are 3 unoccupied orbitals (x,y,z) for each F 1s excitation (localized), of which 1 is lower and 2 are higher in energy. There are 18 F 1s excited states; 6 lower-energy states and 12 higher-energy states. (c) The lower-energy states in the delocalized state picture [corresponding to F 1s $a_{1g} \rightarrow t_{1u}(T_{1u})$ and F 1s $t_{1u} \rightarrow t_{1u}(A_{1g}, E_g)$]. (d) The higher-energy states in the delocalized state picture [corresponding to F 1s $t_{1u} \rightarrow t_{1u}(T_{2g}, T_{1g})$ and F 1s $e_g \rightarrow t_{1u}(T_{1u}, T_{2u})$].

(a)			
Excitation	Energy (eV)	Term value	Oscillator strength
$F+z$ ionization	695.19		
$F+z$ $t_{1u}(z)$	693.73	1.46	6×0.00190
$F+z$ $t_{1u}(x,y)$	694.86	0.33	6×0.00570
(b)			
	Lower	Higher	
	$(Fxx+): F+x \rightarrow t_{1u}(x+)$	$(Fxy+): F+x \rightarrow t_{1u}(y+)$	
	$(Fyy+): F+y \rightarrow t_{1u}(y+)$	$(Fxz+): F+x \rightarrow t_{1u}(z+)$	
	$(Fzz+): F+z \rightarrow t_{1u}(z+)$	$(Fyx+): F+y \rightarrow t_{1u}(x+)$	
	$(Fxx-): F-x \rightarrow t_{1u}(x-)$	$(Fyz+): F+y \rightarrow t_{1u}(z+)$	
	$(Fyy-): F-y \rightarrow t_{1u}(y-)$	$(Fzx+): F+z \rightarrow t_{1u}(x+)$	
	$(Fzz-): F-z \rightarrow t_{1u}(z-)$	$(Fzy+): F+z \rightarrow t_{1u}(y+)$	
		$(Fxy-): F-x \rightarrow t_{1u}(y-)$	
		$(Fxz-): F-z \rightarrow t_{1u}(z-)$	
		$(Fyx-): F-y \rightarrow t_{1u}(x-)$	
		$(Fyz-): F-y \rightarrow t_{1u}(z-)$	
		$(Fzx-): F-z \rightarrow t_{1u}(x-)$	
		$(Fzy-): F-z \rightarrow t_{1u}(y-)$	
(c)			
	$T_{1u}(x) = (Fxx+) - (Fxx-)$ $T_{1u}(y) = (Fyy+) - (Fyy-)$ $T_{1u}(z) = (Fzz+) - (Fzz-)$ $A_{1g} = \{(Fxx+) + (Fxx-)\} + \{(Fyy+) + (Fyy-)\} + \{(Fzz+) + (Fzz-)\}$ $E_g(x^2 - y^2) = \{(Fxx+) + (Fxx-)\} - \{(Fyy+) + (Fyy-)\}$ $E_g(z^2) = -\{(Fxx+) + (Fxx-)\} - \{(Fyy+) + (Fyy-)\} + 2\{(Fzz+) + (Fzz-)\}$		
(d)			
	$T_{2g}(xy) = \{(Fxy+) - (Fxy-)\} + \{(Fyx+) - (Fyx-)\}$ $T_{2g}(xz) = \{(Fxz+) - (Fxz-)\} + \{(Fzx+) - (Fzx-)\}$ $T_{2g}(yz) = \{(Fyz+) - (Fyz-)\} + \{(Fzy+) - (Fzy-)\}$ $T_{1g}(xy) = \{(Fxy+) - (Fxy-)\} - \{(Fyx+) - (Fyx-)\}$ $T_{1g}(xz) = \{(Fxz+) - (Fxz-)\} - \{(Fzx+) - (Fzx-)\}$ $T_{1g}(yz) = \{(Fyz+) - (Fyz-)\} - \{(Fzy+) - (Fzy-)\}$ $T_{1u}(x) = \{(Fyx+) + (Fyx-)\} + \{(Fzx+) + (Fzx-)\}$ $T_{1u}(y) = \{(Fxy+) + (Fxy-)\} + \{(Fzy+) + (Fzy-)\}$ $T_{1u}(z) = \{(Fxz+) + (Fxz-)\} + \{(Fyz+) + (Fyz-)\}$ $T_{2u}(x) = \{(Fyx+) + (Fyx-)\} - \{(Fzx+) + (Fzx-)\}$ $T_{2u}(y) = \{(Fxy+) + (Fxy-)\} - \{(Fzy+) + (Fzy-)\}$ $T_{2u}(z) = \{(Fxz+) + (Fxz-)\} - \{(Fyz+) + (Fyz-)\}$		

F 1s orbitals to all four virtual valence orbitals because promotions can occur from both gerade ($2a_{1g}, 1e_g$) and ungerade ($1t_{1u}$) F 1s MOs, as required to fulfill dipole selection rules (Table I).

The term values for the nondipole S 2s features are in reasonable agreement with those reported for the S 1s spectrum and with the term values for their dipole counterparts in the S 2p spectrum (see Table VIII). The F 1s term value differ significantly from the S 2p, S 2s, and S 1s term values, consistent with differing core hole relaxation effects

when the site of the core hole changes.

IV. SUMMARY

Energy-loss spectra of SF₆ have been recorded under near-dipole and strongly nondipole conditions in the region of S 2p, S 2s, and F 1s excitation. The nondipole S 2s states of SF₆ have been identified more clearly than in earlier studies. The F 1s spectral shape was found to be independent of momentum transfer and similar to the optical spectrum,

TABLE VIII. Comparison of term values for S $2p$, S $2s$, S $1s$, and F $1s$ core excitations.

Upper orbital	Experimental core excitation				TV	Calculation		Negative-ion states	
	S $2p^a$	S $2s$	S $1s^b$	F $1s$		<i>ab initio</i> ^c	Z+1 ^d	EA ^e	Δ^f
a_{1g}	8.1	7.4	8.1	6.6	7.5(5)	7.6	7.1	2.5(1)	10.0(6)
t_{1u}	1.8 ^g	4.2	4.1	2.2	2.6(15)	1.9	1.8	7.0(2)	9.6(17)
t_{2g}	-3.1	-2.2	h	-4.3	3.2(6)	-2.7		11.9(1)	15.1(7)
e_g	-15.2	-14.2	h	-17.5		-14.1			

^aAverage of S $2p_{3/2}$ and S $2p_{1/2}$ values.

^bFrom Ref. [21].

^c*Ab initio*, this work. Equally weighted average of term values for all singlet and triplet states.

^dFrom *ab initio* calculation [69] (GAUSSIAN, using the Z+1 approximation).

^eElectron affinity from electron transmission spectroscopy [65].

^fDifference between electron affinity (EA) [65] and the average core excitation term value. This has been suggested as a useful parameter in checking assignments. Values around 8 eV were found in haloethanes [73].

^gAverage energy of the features assigned to the states we attribute to the T_{2g} and E_g associated with the (S $2p^{-1}, t_{1u}$) configuration. Note that the term value for the lower energy (177 eV) t_{1u} feature is 3.6 eV, in better agreement with the term values for the t_{1u} feature in the S $2s$ and S $1s$ spectra.

^hFeatures were attributed to S $1s$ excitations to these orbitals in early work, but photoemission partial cross-section studies [69] suggest the continuum features so assigned are actually shake-up features. No nondipole ISEELS has been carried out in the S $1s$ region.

indicating that F $1s$ excitation is dipole dominated under all conditions examined. The existence of a previously noted [26] nondipole S $2p$ electronic excitation around 181 eV has been confirmed. Its momentum transfer and impact energy dependence, along with a curve fit analysis, strongly suggest that it corresponds to several quadrupole excitations, which have been assigned as the T_{2g} and E_g states associated with the (S $2p^{-1}, t_{1u}$) configuration. *Ab initio* calculations support assignment of the weak dipole signal at 177 eV to the A_{1g} state associated with the (S $2p^{-1}, t_{1u}$) configuration. At increasing momentum transfer, the intensity of the 177-eV feature increases substantially, suggesting that another nondipole-coupled state occurs at this energy.

ACKNOWLEDGMENTS

This research is supported by NSERC (Canada). J.T.F thanks NSERC for financial support. C.C.T thanks CNPq (Brazil) for financial support. We acknowledge helpful and stimulating conversations with Eric Hudson and thank him for permission to use their F $1s$ absorption data for comparison. We thank John Bozek and the other staff of the Advanced Light Source (ALS) for their assistance in recording the S $2s$ optical data. ALS is a national facility supported by the U.S. Department of Energy.

-
- [1] F. A. Cotton and G. Wilkinson, *Advanced Inorganic Chemistry*, 3rd ed. (Interscience, Toronto, 1988), p. 509.
- [2] R. d'Agostino and D. L. Flamm, *J. Appl. Phys.* **52**, 162 (1981).
- [3] R. Pinto, K. V. Ramanathan, and R. S. Babu, *J. Electrochem. Soc.* **134**, 165 (1987).
- [4] T. Urisu and H. Kyuragi, *J. Vac. Sci. Technol. B* **5**, 1436 (1987).
- [5] D. C. Frost, C. A. McDowell, J. S. Sandhu, and D. A. Vroom, *J. Chem. Phys.* **46**, 2008 (1967).
- [6] B. M. Addison-Jones, K. H. Tan, G. M. Bancroft, and F. Cerina, *Chem. Phys. Lett.* **129**, 468 (1986).
- [7] B. M. Addison-Jones, K. H. Tan, B. W. Yates, J. N. Cutler, G. M. Bancroft, and J. S. Tse, *J. Electron Spectrosc. Relat. Phenom.* **48**, 155 (1989).
- [8] V. H. Dibeler and J. A. Walker, *J. Chem. Phys.* **44**, 4405 (1966).
- [9] R. N. Compton, R. H. Huebner, P. W. Reinhardt, and L. G. Christophorou, *J. Chem. Phys.* **48**, 901 (1968).
- [10] D. M. P. Holland, D. A. Shaw, A. Hopkirk, M. A. MacDonald, and S. M. McSweeney, *J. Phys. B* **25**, 4823 (1992).
- [11] T. A. Ferret, D. W. Lindle, P. A. Heimann, M. N. Piancastelli, P. H. Kobrin, H. G. Kerkhoff, U. Becker, W. D. Brewer, and D. A. Shirley, *J. Chem. Phys.* **89**, 4726 (1988).
- [12] V. I. Nefedov, *J. Struct. Chem.* **11**, 272 (1970).
- [13] M. Nakamura, Y. Morioka, T. Hayaishi, E. Ishigura, and M. Sasanuma (unpublished).
- [14] R. E. LaVilla, *J. Chem. Phys.* **57**, 899 (1972).
- [15] D. Blechschmidt, R. Haensel, E. E. Koch, U. Nielsen, and T. Sagawa, *Chem. Phys. Lett.* **14**, 33 (1972).
- [16] J. L. Dehmer, *J. Chem. Phys.* **56**, 4496 (1972).
- [17] A. S. Vinogradov and T. M. Zimkina, *Opt. Spectrosc.* **32**, 17 (1972).
- [18] E. S. Gluskin, A. A. Krasnoperova, and L. N. Mazalov, *J. Struct. Chem.* **18**, 156 (1977).
- [19] M. M. Gofman, V. I. Nefedov, V. L. Kraizman, and R. V. Vedrinski, *J. Electron Spectrosc.* **32**, 59 (1983).
- [20] J. S. Tse and Z. F. Liu, *Phys. Rev. A* **44**, 7838 (1991).
- [21] C. Reynaud, S. Bodeur, J. L. Marechal, D. Bazin, P. Millie, I. Nenner, U. Rockland, and H. Baumgärtel, *Chem. Phys.* **166**, 411 (1992).
- [22] E. Hudson, D. A. Shirley, M. Domke, G. Remmers, A. Puschmann, T. Mandel, C. Xue, and G. Kaindl, *Phys. Rev. A* **47**, 361 (1993).

- [23] T. Sakae, S. Sumiyoshi, E. Murakami, Y. Matsumoto, K. Ishibashi, and A. Katase, *J. Phys. B* **22**, 1385 (1989).
- [24] A. P. Hitchcock, C. E. Brion, and M. J. Van der Wiel, *J. Phys. B* **11**, 3245 (1978).
- [25] A. P. Hitchcock and C. E. Brion, *Chem. Phys.* **33**, 55 (1978).
- [26] I. Harrison, Ph.D. thesis, University of Manchester, 1986 (unpublished).
- [27] K. H. Sze and C. E. Brion, *Chem. Phys.* **140**, 439 (1990).
- [28] J. F. Ying, C. P. Mathers, and K. T. Leung, *Phys. Rev. A* **47**, R5 (1993).
- [29] V. P. Sachenko, E. V. Polozhentsev, A. P. Kovtun, Yu. F. Migal, R. V. Vedrinski, and V. V. Kolesnikov, *Phys. Lett.* **48A**, 169 (1974).
- [30] R. V. Vedrinskii, A. P. Kovtun, V. V. Kolesnikov, Yu. F. Migal, E. V. Polozhentsev, and V. P. Sachenko, *Bull. Acad. Sci. USSR Phys. Ser.* **38**, 8 (1974).
- [31] R. V. Vedrinskii and V. L. Kraizman, *Bull. Acad. Sci. USSR Phys. Ser.* **40**, 114 (1976).
- [32] Yu. F. Migal, *J. Struct. Chem.* **17**, 350 (1976).
- [33] H. Nakamatsu, T. Mukoyama, and H. Adachi, *Chem. Phys.* **143**, 221 (1990).
- [34] R. Tang and J. Callaway, *J. Chem. Phys.* **84**, 6854 (1986).
- [35] H. Nakamatsu, T. Mukoyama, and H. Adachi, *J. Chem. Phys.* **95**, 3167 (1991).
- [36] F. A. Gianturco, C. Guidotti, and U. Lamanna, *J. Chem. Phys.* **57**, 840 (1972).
- [37] P. J. Hay, *J. Am. Chem. Soc.* **99**, 1013 (1977).
- [38] N. Kosugi, S. Bodeur, and A. P. Hitchcock, *J. Electron Spectrosc.* **51**, 103 (1990).
- [39] M. B. Robin, *Chem. Phys. Lett.* **119**, 33 (1985).
- [40] F. Keller and H. Lefebvre-Brion, *Z. Phys. D* **4**, 15 (1986).
- [41] S. Bodeur, I. Nenner, and P. Millie, *Phys. Rev. A* **34**, 2986 (1986).
- [42] J. D. Bozek, K. H. Tan, G. M. Bancroft, and J. S. Tse, *Chem. Phys. Lett.* **138**, 33 (1987).
- [43] J. S. Tse, Z. F. Liu, J. D. Bozek, and G. M. Bancroft, *Phys. Rev. A* **39**, 1791 (1989).
- [44] S. Bodeur, P. Millie, and I. Nenner, *Phys. Rev. A* **41**, 252 (1990).
- [45] G. R. Wight, C. E. Brion, and M. J. Van der Wiel, *J. Electron Spectrosc.* **1**, 457 (1972).
- [46] A. P. Hitchcock and C. E. Brion, *J. Electron Spectrosc.* **18**, 1 (1980).
- [47] J. L. Dehmer and D. Dill, *Phys. Rev. Lett.* **35**, 213 (1975).
- [48] D. Dill, *J. Chem. Phys.* **65**, 5327 (1976).
- [49] J. L. Dehmer, A. C. Parr, and S. H. Southworth, in *Handbook on Synchrotron Radiation*, edited by G. V. Marr (North-Holland, Amsterdam, 1987), Vol. 2, Chap. 5.
- [50] J. A. Sheehy, T. J. Gil, C. L. Winstead, R. E. Farren, and P. W. Langhoff, *J. Chem. Phys.* **91**, 1796 (1989).
- [51] J. Stöhr, *NEXAFS Spectroscopy*, Springer Series in Surface Sciences Vol. 25 (Springer-Verlag, Heidelberg, 1992).
- [52] M. B. Robin, *Higher Excited States of Polyatomic Molecules Vols. 1-3* (Academic Press, 1974, 1985).
- [53] W. H. E. Schwarz, T. C. Chang, U. Seeger, and K. H. Hwang, *Chem. Phys.* **117**, 73 (1987).
- [54] C. C. Turci, J. T. Francis, T. Tyliczszak, G. G. B. de Souza, and A. P. Hitchcock, following paper, *Phys. Rev. A* **52**, 4678 (1995).
- [55] A. P. Hitchcock, *Phys. Scr.* **T31**, 159 (1990).
- [56] R. N. S. Sodhi and C. E. Brion, *J. Electron Spectrosc.* **34**, 363 (1984).
- [57] N. Kosugi and H. Kuroda, *Chem. Phys. Lett.* **74**, 490 (1980).
- [58] N. Kosugi, *Theoret. Chim. Acta* **72**, 149 (1987).
- [59] P. S. Bagus and H. F. Schaefer III, *J. Chem. Phys.* **56**, 224 (1972); N. Kosugi, E. Shigemasa, and A. Yagishita, *Chem. Phys. Lett.* **190**, 481 (1992).
- [60] S. Huzinaga, J. Andzelm, M. Klobukowski, E. Radzio-Andzelm, Y. Sakai, and H. Tatewaki, *Gaussian Basis Sets for Molecular Calculations* (Elsevier, Amsterdam, 1984).
- [61] N. Rösch, V. H. Smith, Jr., and M. H. Whangbo, *J. Am. Chem. Soc.* **96**, 5984 (1974).
- [62] G. L. Gutsev and A. P. Klyagina, *Chem. Phys.* **75**, 243 (1983).
- [63] W. L. Jolly, K. D. Bomben, and C. J. Eyermann, *At. Data Nucl. Data Tables* **31**, 433 (1984).
- [64] R. W. Shaw, Jr., T. X. Caroll, and T. D. Thomas, *J. Am. Chem. Soc.* **95**, 5870 (1973).
- [65] R. E. Kennerly, R. A. Bonham, and M. McMillan, *J. Chem. Phys.* **70**, 2039 (1979).
- [66] J. T. Francis, C. Enkvist, S. Lunell, and A. P. Hitchcock, *Can. J. Phys.* **72**, 879 (1994); J. T. Francis, N. Kosugi, and A. P. Hitchcock, *J. Chem. Phys.* **101**, 10 429 (1994).
- [67] A. Niehaus, *J. Phys. B* **10**, 1845 (1977).
- [68] T. A. Ferrett, D. W. Lindle, P. A. Heimann, H. G. Kerkhoff, U. E. Becker, and D. A. Shirley, *Phys. Rev. A* **34**, 1916 (1986).
- [69] J. A. Tossell, *Chem. Phys.* **154**, 211 (1991).
- [70] P. Aebi, M. Erbudak, F. Vanini, D. D. Vvedensky, and G. Kosterz, *Phys. Rev. B* **41**, 11 760 (1990); **42**, 5369 (1990).
- [71] M. De Crescenzi, *CRC Crit. Rev. Solid State Mater. Sci.* **15**, 279 (1989).
- [72] A. P. Hitchcock, *Jpn. J. Appl. Phys. Suppl.* **2** **32**, 176 (1993).
- [73] A. Benitez, J. H. Moore, and J. A. Tossell, *J. Chem. Phys.* **88**, 6691 (1988).
- [74] A. P. Hitchcock and M. Tronc, *Chem. Phys.* **121**, 265 (1988).